Production of a Switchable Fission-like Neutron Flux Using a Monoenergetic 14 MeV Neutron Generator and a Depleted Uranium Reflector for Vehicle Borne Improvised Explosive Device Detection

D. Koltick and S. McConchie

Applied Physics Laboratory, Purdue University, 525 Northwestern Avenue, West Lafayette, IN 47907-2036
koltick@purdue.edu, mcconchi@purdue.edu

A remotely controlled prototype has been built to detect explosives in vehicles. The inspection time is between 2 to 5 minutes. The system utilizes a neutron generator and a ^{238}U reflector as the neutron source and high-purity germanium (HPGe) detectors housed in moving components that scan the entire vehicle. The design and performance of a switchable neutron source utilizing a D-T neutron generator and a depleted uranium reflector are presented. Approximately half the generator's 14 MeV neutron flux is used to produce a fission-like neutron spectrum similar to ^{252}Cf. For every 14 MeV neutron entering the reflector, more than one fission-like neutron is reflected back across the surface of the reflector. The source has pulsed mode capability, because delayed neutron production is two orders of magnitude below prompt neutron production. The source simultaneously emits 14 MeV neutrons optimal to excite fast neutron-induced gamma-ray signals, such as from carbon and oxygen, and fission-like neutrons optimal to induce neutron capture gamma-ray signals, such as from hydrogen, nitrogen, and chlorine. Experiments were performed, which compare well to Monte Carlo simulations, showing that the uranium reflector enhances thermal signals by a factor of 15 compared to the absence of a reflector.

I. INTRODUCTION

Recent times have demonstrated the increasing occurrence of rogue individuals or groups to use large-scale vehicle borne improvised explosive devices (VBIEDs) to create mayhem and effectively disable government and economic functions. The global nature of this threat is exemplified in the well-known bombings of the Oklahoma Federal Building in 1995 and Bali Nightclub in 2002. These bombings involved several hundred to several thousand pounds of explosive and set the scale of the type of attacks that are not aimed at specific individuals but cause widespread negative political and economic impact. The threat scale justifies the use of the highest quality equipment in order to achieve the fastest scan times with reasonable detection rates.

The current concept of operation for VBIED detection calls for physical search by visual inspection of the vehicle, putting personnel at high risk. There are more sophisticated systems that utilize X-ray and vapor detection technologies [1-3]. Most common explosives expected in VBIEDs are nitrogen and oxygen rich [4,5], allowing them to be distinguished easily from innocuous items on this scale using neutron-induced gamma ray spectroscopy. Screening systems which utilize neutron interrogation techniques such as thermal neutron analysis (TNA) [6], gated thermal neutron analysis (GTNA) [7], fast neutron analysis (FNA) [8], pulsed fast neutron analysis (PFNA) [9], pulsed fast-thermal neutron analysis (PFTNA) [10], and associated particle time-of-flight analysis [11] have been developed for numerous applications such as humanitarian demining [12-14], explosive inspection of cargo [15-18], mid-size truck [19], luggage [20-22], UXO identification [23-25], and material characterization [26-27].

We have developed a neutron-based interrogation system to non-intrusively and non-destructively detect VBIEDs in vehicles ranging from compact cars to full-size passenger vans. The system combines the advantages of three methods: TNA, GTNA and FNA. It automatically makes a decision about the presence of a VBIED in 2 to 5 minutes using an easy-to-understand graphic user interface, provides vehicle imaging information, uses commercial off the shelf components, and operates safely for the public, stowaways, and system operator.

II. DESCRIPTION OF THE SYSTEM

The system interrogates a vehicle using a D-T neutron generator operating at 10^8 neutrons per second. The generator emits fast 14 MeV neutrons to penetrate deeply into the vehicle and excite nuclei through inelastic scattering to induce fast gamma-ray signals. In order to enhance the slow neutron flux for slow signals throughout the vehicle a depleted uranium reflector has been coupled with the generator. Generator neutrons emitted away from the vehicle enter the reflector and induce fission neutrons whose energy spectrum is similar to ^{252}Cf. Monte Carlo calculations show that for every 14 MeV neutron entering the reflector more than one fission like neutron with an average energy approximately 2 MeV is emitted in the direction of the vehicle. The generator and

reflector coupling has properties of both a D-T neutron generator and a ^{252}Cf neutron source while still allowing neutron production to be switched on and off.

III. MOTIVATION FOR USING URANIUM

Depleted uranium (DU) is composed of 99.8% ^{238}U, 0.2% ^{235}U, and trace amounts of other heavy elements and has high density at 19.0 g/cc. ^{238}U is a fissionable material whose neutron-induced fission cross-section is 1.14 b at 14 MeV and drops to approximately 0.53 b at 2 MeV [28]. On average, 4.4 neutrons are produced from each fission with a Watt spectrum very similar to that for ^{252}Cf [29]. ^{238}U produces net numbers of neutrons from the (n,2n) and (n,3n) reactions whose cross-sections are 0.87 b and 0.45 b at 14 MeV, respectively. The neutrons emitted from the knockout reactions are not dissimilar to the ^{252}Cf Watt spectrum. All these spectra are compared in Figure 1. The neutrons emitted from fission and knockout reactions have an energy spectrum capable of inducing secondary fission reactions. Thus the fission and neutron-producing reactions within uranium allow it to couple well with a D-T neutron generator, creating a switchable source producing both fission-like neutrons and 14 MeV neutrons of comparable flux.

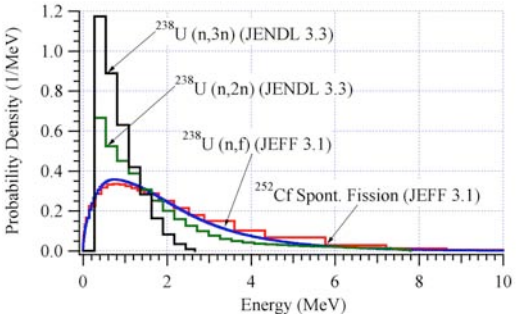

Figure 1. Emitted neutron energy spectrum for ^{238}U from neutron induced fission and ^{252}Cf from spontaneous fission.

^{238}U produces net neutrons when exposed to 14 MeV neutrons. A reflector model was developed whose maximal response produces results that no practical reflector can exceed. This model is a 2 meters × 2 meters × d cm thick rectangular reflector with a 14 MeV isotropic neutron point source placed 5 cm above the center of the reflector. The source placement simulates the typical distance between a neutron generator target plane and the generator's outer housing. MCNP [30] calculated the neutron return across the upper surface of the reflector per source neutron entering as a function of energy. All MCNP tally results had a relative error of less than 0.10.

The neutron return as a function of thickness and energy are shown in Figure 2. The maximum neutron return was 220% for the energy range 0 MeV to 14 MeV. In the range 100 keV to 6 MeV, which is characteristic of ^{252}Cf sources, the maximum neutron return for uranium is 190%. In this energy range, the uranium thickness required for maximum neutron return is 20 cm.

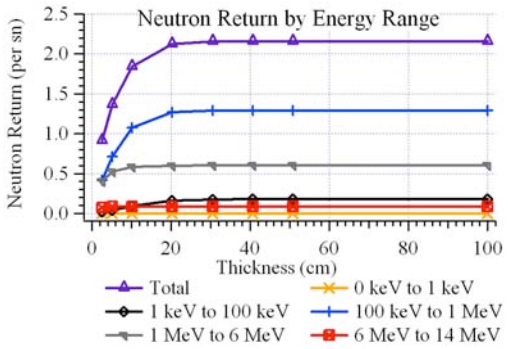

Figure 2. Plots of neutron return per source neutron entering the reflector as a function of thickness and of energy.

IV. NEUTRON REFLECTOR DESIGN

A large planar reflector can be rendered practical by curling the sides into a cylindrical geometry and placing the generator target plane symmetrically on the cylinder axis, as shown in Figure 3. This approach allows two parameters to describe a practical reflector, its length and thickness. While a Monte Carlo simulation selects the optimal parameters, it is useful to develop a simple analytic model in order to understand the physics behind the result.

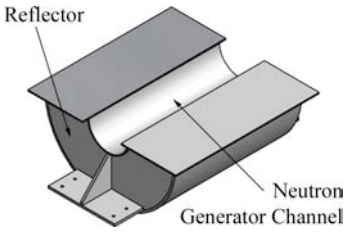

Figure 3. The uranium reflector.

Because ^{238}U is so heavy, the elastically scattered 14 MeV generator neutrons entering the reflector are strongly diffracted forward by individual nuclei, with no energy loss, at an angular half width of 0.2 radians. For this reason, elastic scattering does not control the neutron penetration depth into the reflector. The depth is controlled by the 14 MeV neutron-induced fission, (n,2n), and (n,3n) reactions. The mean free path, λ_n, for neutron production is:

$$\lambda_n = \frac{1}{\rho_N \sum_i \sigma_i}, \qquad (1)$$

where ρ_N is the number density and σ_i is the cross-section for a particular reaction on ^{238}U. At 14 MeV, λ_n = 8.5 cm and is comparable to the mean free path for elastic scattering of $\lambda_{elastic}$ = 7.5 cm.

Because elastic scattering is strongly diffractive at 14 MeV, the number of scattering steps, $N_{elastic}$, required to have a significant portion of the scattered neutrons moving backwards is given by [31]:

$$\sqrt{N_{elastic}}\,\delta\theta \sim \frac{\pi}{2}, \qquad (2)$$

where $\delta\theta$ is diffraction angle. The result is that approximately 10 diffractive scatterings are required before the neutron flux has a significant component moving backward. However, because only one neutron producing reaction is sufficient to greatly alter the incident neutron direction, these reactions control the penetration depth and 14 MeV elastic scattering can be ignored.

Most of the incident neutron flux then has reacted by a depth of λ_n. At this depth, secondary neutron production is capable of inducing fission on ^{238}U. These secondary fission-produced neutrons have a mean energy of ~ 2 MeV and a mean free path of $\lambda_n^{fission}$ = 39.3 cm, and are capable of producing a comparable number of neutrons as the first generation. However, the elastic scattering mean free path for these neutrons is only $\lambda_{elastic}^{fission}$ = 5.1 cm. While these lower energy neutrons are diffractive, their diffraction angle at half width is ~ 1 radian. Thus, because the elastic scattering randomizes the angular distribution, the induced fission neutrons on average have no preferred direction.

Using a three-dimensional random walk calculation to describe the diffusion of these neutrons, the distance traveled, $T_{secondary}$, in terms of the number of steps, $N_{elastic}^{fission}$, and the step size, $\lambda_{elastic}^{fission}$, is:

$$T_{secondary} = \sqrt{N_{elastic}^{fission}}\,\frac{\lambda_{elastic}^{fission}}{\sqrt{3}}. \qquad (3)$$

The total length of the particle path is given by $D = N_{elastic}^{fission}\lambda_{elastic}^{fission} = N_n^{fission}\lambda_n^{fission}$, where $N_n^{fission}$ is the number of steps for neutron production. Equation (3) becomes:

$$T_{secondary} = \sqrt{\frac{1}{3}\left(N_n^{fission}\lambda_n^{fission}\right)\lambda_{elastic}^{fission}}. \qquad (4)$$

The probability, P, for a neutron producing reaction to occur as a function of the number of steps, $N_n^{fission}$, is:

$$P = 1 - e^{-N_n^{fission}} = 1 - \exp\left(-3T_{secondary}^2 / \lambda_n^{fission}\lambda_{elastic}^{fission}\right). \qquad (5)$$

Therefore, the approximate additional reflector thickness required to take into account secondary fissions is:

$$T_{secondary} = \sqrt{\frac{1}{3}\lambda_n^{fission}\lambda_{elastic}^{fission}\ln\left(\frac{1}{1-P}\right)}. \qquad (6)$$

The total thickness then required to produce both 1st and 2nd generation neutrons is then:

$$T = \lambda_n + T_{secondary}. \qquad (7)$$

Using λ_n = 8.5 cm and $T_{secondary}$ = 14.1 cm for P = 95%, the simple model estimates the required thickness to be ~23 cm.

MCNP simulations were conducted to calculate the thickness and length giving maximal neutron return. The MCNP result includes all generations of neutrons produced by previous generations. Using the cylindrical geometry shown in Figure 3, the length was set to 2 m, and the thickness was varied from 1 cm to 30 cm. The neutron return normalized per source neutron entering the reflector as a function of thickness is shown in Figure 4 (a). The neutron return is 95% of the maximum at a thickness of 20.8 cm. This result agrees well with the simplified random walk model. The thickness was then set to 1 m and the length was varied from 2 cm to 60 cm. The neutron return as a function of length is shown in Figure 4 (b). The neutron return is 95% of the maximum at lengths 46.3 cm. Therefore, the optimal reflector is 21 cm thick and 46 cm long.

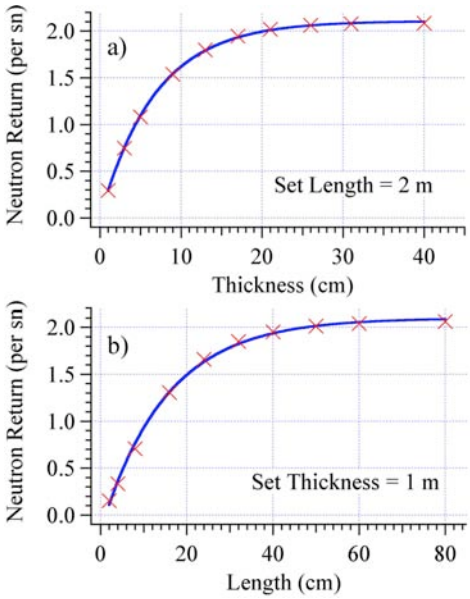

Figure 4. Neutron return for all energies across the top plane of the reflector as a function of the (a) thickness and (b) length.

For portability reasons, the reflector designed for the vehicle scanning system [32] had a maximum weight restricted to 320 kg (700 lbs.). MCNP simulations were conducted to optimize the thickness and length of the reflector for a fixed weight. Using 5 cm as the radius of the neutron generator channel, the thickness and length were each varied such that the total weight remained at 320 kg. The maximum number of reflected neutrons from 100 keV to 6 MeV occurs for a reflector thickness of 10 to 13 cm.

The final reflector is 12.7 cm thick and 37.5 cm long. The neutron generator channel diameter was set to 12.1 cm in order to allow padding for a generator head with a typical diameter of 10 cm. The reflector top was encapsulated in 0.3 cm of 304 stainless steel while all other surfaces were encapsulated with 0.6 cm stainless steel. The reflector was manufactured by Manufacturing Sciences Corporation with a weight of 326.8 kg and density of 18.0 g/cc. Due to the weight limitation, the reflector achieves 60% of the ideal neutron return.

V. NEUTRON AMPLIFICATION SIMULATIONS

The characteristic neutron spectrum of the designed reflector including its steel encapsulation was calculated using MCNP. The neutron return across the top surface of the reflector as a function of energy is shown in Figure 5. In the figure, the neutron return energy spectrum maximizes at 600 keV. The spectrum compares well to a ^{252}Cf fission spectrum, which is also shown. The integration of the reflected neutron spectrum is also shown in Figure 5. The neutron return from 0 MeV to 14 MeV per source neutron entering the reflector is 1.21. The coupling of the neutron generator to the reflector increases or amplifies the number of neutrons moving towards the target by a factor of 2.2.

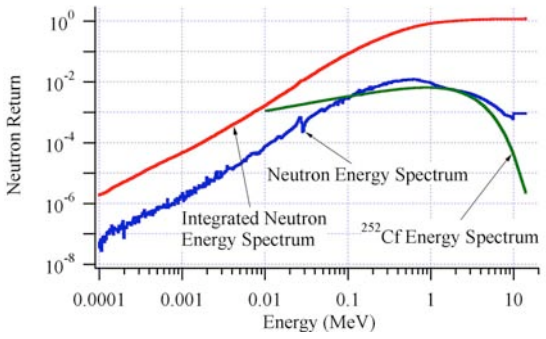

Figure 5. Neutron return as a function of energy across the top surface of the uranium reflector in the final design.

MCNP was also used to calculate the number of fission, (n,2n), and (n,3n) reactions occurring in the reflector. The expected values and simulation results are shown in Table 1. The reaction cross-section, σ, average neutrons emitted from each reaction, $\bar{\upsilon}$, and the product of both, $\sigma\bar{\upsilon}$, are listed. The ratio of the product for each reaction relative to fission is shown. MCNP calculated the reaction rate, *R*, in the reflector for each reaction per source neutron entering the reflector.

The reaction dominating neutron production is fission by a factor of 4 and 6 over (n,2n) and (n,3n), respectively.

Neutron Producing Reaction	MCNP Reaction Rate *R*	MCNP $\bar{\upsilon}$	$R\bar{\upsilon}$	$R\bar{\upsilon}$ Ratio Relative to Fission
Fission	5.2×10^{-1}	3.8	2.0×10^{0}	1.00
(n,3n)	1.0×10^{-1}	3	3.0×10^{-1}	0.16
(n,2n)	2.6×10^{-1}	2	5.2×10^{-1}	0.26

Table 1. Relative contribution of neutron producing reactions on ^{238}U in the designed reflector.

VI. REFLECTOR PERFORMANCE EXPERIMENTAL SET UP

Experimental tests were performed to measure the performance enhancement of the uranium reflector relative to lead, carbon, and no reflector. The goal of the experiment was to measure the thermal neutron induced gamma-ray signal enhancement in a sample as a function of the reflector type. A D-T neutron generator with a reflector was used to irradiate a sample of distilled water with neutrons. HPGe detectors were used to measure the hydrogen gamma-ray return signal from the sample. As shown in Figure 6, the experimental setup consisted of an MF-Physics A-325 D-T neutron generator, 3 Ortec PopTop n-type HPGe detectors with relative efficiencies of 66%, 68%, and 77%, Ortec DSPEC Plus digital processors, Ortec X-Cooler II refrigeration units, lead shielding, a 2-liter high-density polyethylene bottle filled with distilled water, and 3 similarly sized reflectors made of depleted uranium, lead, and graphite.

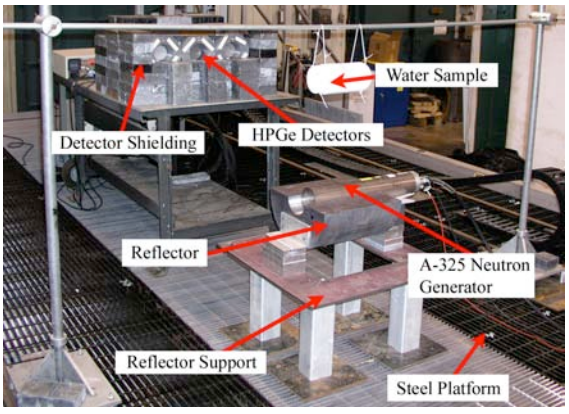

Figure 6. Experimental setup to measure the performance of the uranium reflector in reference to no reflector.

The setup was placed on a steel-grated platform to reduce the gamma-ray background from the floor. The detectors were shielded from the concrete floor by 20 cm of lead shielding and from the rest of the surroundings by at least 15 cm of lead. This limited the hydrogen and oxygen signals in the detectors to those coming from the water sample. Figure 7 shows the hydrogen signal with and without the sample for the uranium reflector, verifying that the detector shielding was sufficient.

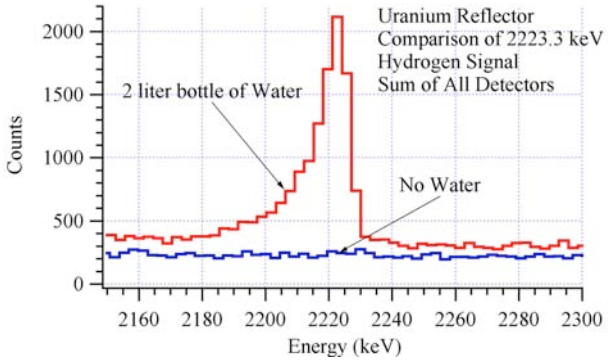

Figure 7. Comparison of hydrogen signal with and without 2-liter bottle of water for the uranium reflector.

The digital processors' pulse shaping parameters were optimized using ^{60}Co and ^{137}Cs check sources. During data acquisition, the neutron generator was operated at 8×10^{7} neutrons per second. The average live singles rate in the detectors for all reflectors during continuous mode operation was 24 kHz with a dead time of 29%. The digital processors collected pulse height spectra with 16384 channels. A linear energy calibration of the detectors was found using the 511 keV annihilation line, 1332.5 keV ^{60}Co line, and 2614.5 keV ^{208}Pb line.

The 2223.3 keV gamma-ray from the ^{1}H(n,γ) reaction in the sample was used to determine the relative reflector performance. This signal was collected in pulsed mode to improve its signal-to-noise ratio. In pulsed mode, the neutron generator was operated with a 10 kHz pulse frequency and 15% duty factor, resulting in a 100 μs total cycle length and 15 μs neutron pulse length. The detectors were gated so that data were collected from 25 μs to 100 μs. Data were acquired for 5 minutes of live time in pulsed mode to detect hydrogen.

The various hydrogen signals are shown in Figure 8. Performing a guard band count analysis on each detector's spectrum, the total hydrogen signal for each reflector type was corrected for the live count rate differences between the reflectors. The hydrogen signal counts and errors are given in Table 2. To verify the generator stability between data acquisition runs, the generator was operated in continuous mode for 20 minutes live time to collect the ^{16}O inelastic scattering gamma-ray signal from the water sample. This signal is sensitive only to the neutrons emitted from the generator and not those from the reflector. The oxygen signal counts over the course of the experiment were constant within error and verifies the generator stability.

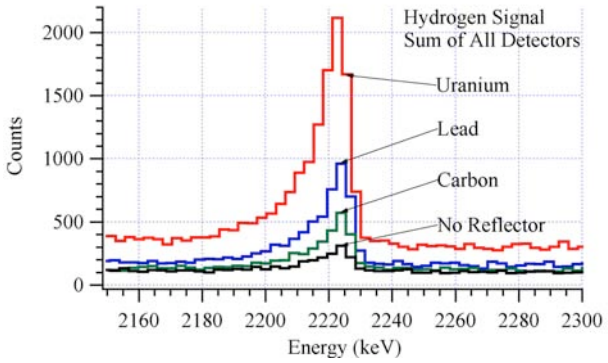

Figure 8. Hydrogen signal for the uranium, lead, carbon, and no reflectors.

	Experimental Results	
Reflector	Hydrogen Counts	Thermal Capture Die-away (μs)
Uranium	8429.4 ± 121.9	96.9 ± 3.4
Lead	3490.3 ± 78.7	89.0 ± 4.8
Carbon	1825.9 ± 60.4	98.1 ± 8.0
None	699.9 ± 37.6	83.2 ± 4.7
	Experimental Results	
	Relative Pulsed Correction	Improvement Factor
Uranium	1.188 ± 0.085	14.31 ± 1.29
Lead	1.082 ± 0.092	5.39 ± 0.55
Carbon	1.204 ± 0.130	3.14 ± 0.39
None	1.000 ± 0.084	1.00 ± 0.08
	MCNP Results	
	Hydrogen Capture Rate	Improvement Factor
Uranium	6.84×10^{-7} ± 5.2%	15.32 ± 1.11
Lead	2.58×10^{-7} ± 9.3%	5.77 ± 0.61
Carbon	1.12×10^{-7} ± 5.5%	2.50 ± 0.19
None	4.47×10^{-8} ± 5.0%	1.00 ± 0.07

Table 2. Experimental and Monte Carlo results for the improvement factor in reference to no reflector.

VII. PULSED MODE CORRECTION

A correction to the hydrogen counts observed for the reflector must be considered, because the detectors are not collecting data during the full cycle in pulsed mode. The reflector has a different correction than the no reflector case due to the variation in the neutron energy spectrum

and the neutron leakage rate from the reflector. Therefore, the number of gamma rays observed from thermal neutron capture during the detector gate will vary depending upon the characteristic die-away time in the sample. To estimate the total neutron flux using the observed hydrogen signal, the counts must be corrected using the die-away time constant to take into account the detector off time during the cycle. A correction is not required in continuous mode operation, because the neutron flux in the sample reaches a steady state for each reflector, and the detectors are not gated.

In order to determine the correction, consider the rate at which thermal neutron captures occur within the sample. During the detector gate when the neutron generator is off, the thermal neutron capture activity decays exponentially with a characteristic decay time. Letting w be the total cycle time, the number of captures, $\Delta N_{0\to i}$, occurring in the gate including those from all previous neutron pulses i yields the total number of captures occurring in the gate, ΔN_{total}, due to all previous gates, is:

$$\begin{aligned}\Delta N_{total} &= \lim_{n\to\infty}\sum_{i=0}^{n}\Delta N_i \\ &= A_0\tau\exp\left(-t_1/\tau\right)\frac{\left(1-\exp\left(-\Delta t/\tau\right)\right)}{\left(1-\exp\left(-w/\tau\right)\right)},\end{aligned} \tag{8}$$

The relative performance of the uranium reflector compared to no reflector is given by:

$$\frac{\tau_{\text{Reflector}}\exp\left(-t_1/\tau_{\text{Reflector}}\right)\left(1-\exp\left(-\Delta t/\tau_{\text{Reflector}}\right)\right)\left(1-\exp\left(-w/\tau_{\text{None}}\right)\right)}{\tau_{\text{None}}\exp\left(-t_1/\tau_{\text{None}}\right)\left(1-\exp\left(-\Delta t/\tau_{\text{None}}\right)\right)\left(1-\exp\left(-w/\tau_{\text{Reflector}}\right)\right)} \tag{9}$$

This result requires the measurement of the characteristic time for the neutron die-away within the sample due to each reflector type.

The characteristic time was measured by setting the pulse frequency to 2.5 kHz such that the total pulse length was 400 µs. For an estimated characteristic time of 100 µs, the selected pulse length allows the thermal neutron capture rate to decay 5 half-lives and the residual capture overlap becomes negligible. The thermal capture die-away times for each reflector are shown in Table 2.

The resulting pulsed mode corrections and improvement factors are shown in Table 2. The error in the hydrogen counts includes the error contributions from Equation (9), which were calculated using a Monte Carlo program. The improvement factor for uranium over no reflector was observed to be (14.31 ± 1.29), and the uranium reflector outperformed the lead reflector by a factor of 2.7. These improvement factors have been verified with Monte Carlo simulations using MCNP.

VIII. VERIFICATION OF THE EXPERIMENTAL TESTS WITH MONTE CARLO SIMULATIONS

The experimental geometry, shown in Figure 6, was simulated using MCNP. MCNP calculated the number of hydrogen captures occurring in the 2-liter water sample for each reflector. The improvement factor is the hydrogen signal for each reflector compared to the case of no reflector. The Monte Carlo program predicts the improvement factor to be (15.3 ± 1.1), which agrees well with the experimental result of (14.3 ± 1.3) in Table 2. The comparison of the experiment to the Monte Carlo results for all reflectors are shown in Figure 9.

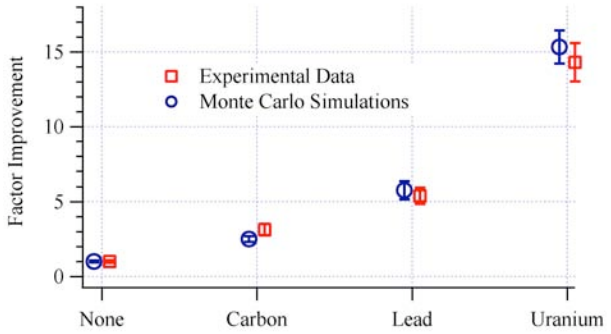

Figure 9. Improvement factor of uranium, lead, and carbon reflectors compared to no reflector.

IX. REFLECTOR DELAYED NEUTRON PRODUCTION

MCNP calculations were conducted to characterize the neutron return as a function of time. The reflector's neutron die-away is shown in Figure 10. The neutron flux reduces by two orders of magnitude at 1 µs after generator neutron production ceases. As a result, the neutron flux from the reflector is pulseable on megahertz time scales.

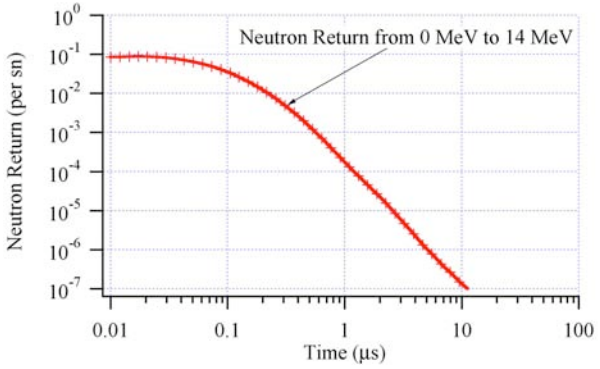

Figure 10. Neutron return through the top surface per source neutron entering the reflector at t=0 as a function of time after the neutron generator has been turned off.

However, there is neutron production due to delayed neutrons from induced fission fragments after the generator is turned off. Delayed neutron precursors are organized into six groups based on their similar half-lives that decay exponentially with time, as shown in Table 3 [33]. During the irradiation period, the number of delayed neutron precursors asymptotically increases within the uranium reflector until the number of delayed neutron precursors being created is equivalent to the number of precursors decaying. The asymptotic neutron flux is calculated using the induced fission rate in the reflector and the number of delayed neutrons per fission, $\upsilon_d = 0.0412$ for ^{238}U [33].

Group	Half-life (s)	Relative Abundance
1	52.38	0.013
2	21.58	0.137
3	5.00	0.162
4	1.93	0.388
5	0.49	0.225
6	0.17	0.075

Table 3. Delayed neutron precursor groups for ^{238}U. Delayed neutron production due to uranium fission is characterized by a large number of neutron precursors which can be separated into six groups based on their similar half-lives which decay exponentially with time.

The ratio of the generator pulse-off to pulse-on neutron production is given by:

$$\frac{\upsilon_d R_f}{1+\sum_i R_i \overline{\upsilon_i}} \qquad (10)$$

where R_f is the induced fission rate, R_i is the reaction rate for each type of neutron production reaction, and $\overline{\upsilon_i}$ is the average number of neutrons produced. All three parameters are unique to the reflector. The induced fission rate was calculated to be 0.26 fissions per source neutron using MCNP. In Equation (10), the denominator has two neutron source terms. The first term represents the generator and the second term represents the reflector response. The reflector response term is calculated using the results from Table 1 to be 2.8. The neutron production off to on ratio is ~2.8×10^{-3}.

X. CONCLUSIONS

A neutron source has been developed that simultaneously emits 14 MeV neutrons optimal to excite fast neutron-induced gamma-ray signals, such as from carbon and oxygen, and a comparable strength fission-like neutron spectrum optimal to induce neutron capture gamma-ray signals, such as from hydrogen, nitrogen, and chlorine. The source is capable of pulse-mode operation up to megahertz frequencies because the ratio of the generator pulse-off to pulse-on is only ~$3\cdot10^{-3}$.

ACKNOWLEDGMENTS

The authors acknowledge the support of this work by Naval Surface Warfare Center, Dahlgren, Naval Surface Warfare Center, Crane, and U.S. Army support provided through Argonne National Laboratory.

REFERENCES

1. A.V. Kuznetsov, in Proceedings of the NATO Advanced Research Workshop on Detection of Bulk Explosives, Advanced Techniques against Terrorism (2003) 7-30.
2. S. Singh and M. Singh, Signal Processing 83 (2003) 31-55.
3. M. Krausa, in Proceedings of the NATO Advanced Research Workshop on Detection of Bulk Explosives, Advanced Techniques against Terrorism (2003) 31-37.
4. P. Shea and T. Gozani, in Proceedings of Nuclear Techniques for Analytical and Industrial Applications (1992) 359-379.
5. G. Vourvopoulos, Chemistry and Industry (1994) 297-300.
6. P. M. Shea *et al.*, Nuclear Instruments and Methods in Physics Research A 299 (1990) 444.
7. P. Womble *et al.*, Nuclear Instruments and Methods in Physics Research B 99 (1995) 757.
8. L. Zhang and R. Lanza, in Nuclear Science Symposium 1 (1998) 353-355.
9. J. Rynes *et al.*, Nuclear Instruments and Methods in Physics Research A 422 (1999) 895.
10. T. Gozani, in Proceedings of SPIE 2936 (1996) 9-20.
11. A. Beyerle *et al.*, Nuclear Instruments and Methods in Physics Research A 299 (1990) 458.
12. G. Vesti *et al.*, Nuclear Instruments and Methods in Physics Research A 422 (1999) 918.
13. F. D. Brooks *et al.*, Applied Radiation and Isotopes 61 (2004) 27-34
14. G. Vourvopoulos and P. Womble, Talanta 54 (2001) 459-468.
15. S. Khan, in Proceedings of SPIE 2276 (1994) 294-309.
16. T. Gozani, in Proceedings of SPIE 2867 (1997) 174-181.
17. A. Barzilov *et al.*, in AIP Conference Proceedings 680 (2003) 939-942.
18. D. R. Brown, in Proceeding of SPIE 2092 (1994) 254-262.
19. E. L. Reber *et al.*, Nuclear Instruments and Methods in Physics Research B 241 (2005) 738.

20. J. H. Flexman *et al.*, in Proceedings of the NATO Advanced Research Workshop on Detection of Bulk Explosives, Advanced Techniques against Terrorism (2003) 113-124.
21. J. C. Overley *et al.*, in Proceedings of SPIE 2867 (1997) 219-222.
22. T. Gozani *et al.*, Nuclear Instruments and Methods in Physics Research Section A 299 (1990) 444.
23. P. Womble *et al.*, Proceedings of SPIE 4786 (2002) 52057.
24. C. Bruschini, Subsurface Sensing Technologies and Applications 2 (2001) 299-336.
25. W. E. Parket *et al.*, in Proceedings of SPIE 3769 (1999) 43-50.
26. M. Belbot *et al.*, in Proceeding of SPIE 3769 (1999) 168-177.
27. P. Womble et al., Nuclear Instruments and Methods in Physics Research B 241 (2005) 765.
28. Neutron-induced reaction file (Comp. and Ed.) P.F. Rose: "ENDF-201, ENDF/B-VI Summary Documentation," BNL-NCS-17541, 4th Edition (1991).
29. J. Terrell, Phys. Rev. 113 (1959) 527.
30. R. Forster et al., Nucl. Instr. and Meth. B 213 (2004) 82.
31. M. Blann and M.B. Chadwick, Phys. Rev. C 57 (1998) 233.
32. D. Koltick et al., Nucl. Instr. and Meth. B (2007), doi:101016/j.nimb.2007.03.047.
33. J.R. Keepin et al., Phys. Rev. 107 (1957) 1044.